Combustion and Flame 157 (2010) 556–565

Contents lists available at ScienceDirect

Combustion and Flame

journal homepage: www.elsevier.com/locate/combustflame

Formation and consumption of NO in $H_2 + O_2 + N_2$ flames doped with NO or NH_3 at atmospheric pressure

A.G. Shmakov [a,*], O.P. Korobeinichev [a,b], I.V. Rybitskaya [a,b], A.A. Chernov [a], D.A. Knyazkov [a], T.A. Bolshova [a], A.A. Konnov [c]

[a] Institute of Chemical Kinetics and Combustion, Novosibirsk, Russian Federation
[b] Novosibirsk State University, Novosibirsk, Russian Federation
[c] Division of Combustion Physics, Lund University, Lund, Sweden

ARTICLE INFO

Article history:
Received 19 June 2009
Received in revised form 14 October 2009
Accepted 15 October 2009
Available online 24 November 2009

Keywords:
Hydrogen
Flame structure
Nitrogen oxides
Molecular-beam mass spectrometry

ABSTRACT

Flat premixed burner-stabilized $H_2 + O_2 + N_2$ flames, neat or doped with 300–1000 ppm of NO or NH_3, were studied experimentally using molecular-beam mass-spectrometry and simulated numerically. Spatial profiles of temperature and concentrations of stable species, H_2, O_2, H_2O, NO, NH_3, and of H and OH radicals obtained at atmospheric pressure in lean ($\phi = 0.47$), near-stoichiometric ($\phi = 1.1$) and rich ($\phi = 2.0$) flames are reported. Good agreement between measured and calculated structure of lean and near-stoichiometric flames was found. Significant discrepancy between simulated and measured profiles of NO concentration was observed in the rich flames. Sensitivity and reaction path analyses revealed reactions responsible for the discrepancy. Modification to the model was proposed to improve an overall agreement with the experiment.

1. Introduction

Due to massive research efforts made in the last two–three decades, major reactions of nitrogen chemistry in flames are now well understood. Considerable progress has been achieved in the development of detailed kinetic mechanisms describing NO_x formation and reburning in natural gas combustion, for instance GRI-mechanism [1]. In most cases the GRI-mech. predictions are in good quantitative or at least in qualitative agreement with new experimental results obtained since its last release. However, some experimental data on ammonia and nitric oxide conversion in premixed flames cannot be reproduced by contemporary kinetic schemes. Knyazkov et al. [2] studied formation and destruction of nitric oxide in methane flames doped with NO at atmospheric pressure. Previously unknown phenomenon, lean reburning of NO in premixed flames, was revealed. Neither the GRI-mech. [1], nor the Konnov detailed reaction mechanism [3] were able to reproduce this observation. Konnov et al. [4] measured concentrations of NO in $(CH_4 + NH_3) + O_2 + N_2$ flames and found satisfactory agreement between experiments and modeling in lean flames. In rich mixtures, however, NO measurements were significantly over-predicted by the mechanisms of Konnov [3] or of Skreiberg et al. [5]. In both cases [2,4] it was concluded that significant qualitative discrepancy between the experiments and modeling is probably due to missing (unknown) reactions and not due to wrong rate constants.

To narrow the search for deficiencies in the kinetic (sub-)mechanisms, experimental data on flame structure of lean hydrogen flames doped with NO and of rich hydrogen flames doped with NH_3 at atmospheric pressure could be most helpful. Regrettably, flame structure studies of formation and consumption of NO in neat or doped with NO or NH_3 hydrogen flames do not cover complete range of interest. Available experimental results obtained in premixed hydrogen flames at various conditions are summarized in Table 1.

NO formation in lean ($\phi = 0.71$) $H_2 + O_2 + N_2$ flames at atmospheric pressure was first studied by Homer and Sutton [6]. Varying concentrations of nitrogen in these flames allowed for different final flame temperatures. Spatial profiles of NO were analyzed taking into account only thermal Zeldovich mechanism of NO formation and super-equilibrium concentrations of O atoms. These results have been revisited by Konnov [7], who demonstrated that NNH route of NO formation is dominant in lean hydrogen flames below ~2000 K. The modeling using detailed H/N/O reaction mechanism [8] was found in satisfactory agreement with the measurements, and strongly supported the new rate constant of NNH radicals' oxidation [9].

The goal of the low pressure experiments of Harrington et al. [10] was to find an evidence for the NNH route of NO production proposed by Bozzelli and Dean [11]. Concentrations of NO and

* Corresponding author. Address: Institute of Chemical Kinetics and Combustion, Institutskaya str. 3, Novosibirsk 630090, Russian Federation. Fax: +7 383 3307350.
E-mail address: shmakov@kinetics.nsc.ru (A.G. Shmakov).

0010-2180/$ - see front matter © 2009 The Combustion Institute. Published by Elsevier Inc. All rights reserved.
doi:10.1016/j.combustflame.2009.10.008

Table 1
Experimental studies of NO formation and consumption in premixed hydrogen flames.

Flame composition	Pressure	Additive	Stoichiometry	Method	Reference
$H_2 + O_2 + N_2$	1 atm	–	0.71	Gas sampling	[6]
$H_2 + O_2 + N_2$	1 atm	–	0.75, 1.5	Gas sampling	[13]
$H_2 + O_2 + N_2$	38, 78 Torr	–	1.5	LIF	[10]
$H_2 + O_2 + Ar$	1 atm	0.1% CH_3CN	1.5–2.6	LIF	[14]
$H_2 + O_2 + Ar$	76 Torr	~0.4, 0.8% NO	0.88–1.5	LIF	[15]
$H_2 + O_2 + Ar$	76 Torr	~0.4, 0.8% NO	0.88–1.74	MBMS	[16]
$H_2 + O_2 + Ar$	1 atm	0.17% NO	1.6	Gas sampling	[17]
$H_2 + O_2 + Ar$	1 atm	~0.2% NO, ~0.2% NH_3	0.8–0.86	Gas sampling	[18]
$H_2 + O_2 + N_2$	1 atm	0.2% NO	0.6–1.0	CRDS, LIF	[19]
$H_2 + O_2 + Ar$	1 atm	0.5% NH_3	1.0	MBMS	[21]
$H_2 + O_2 + Ar$	34.5 Torr	3.4% NO, 3.4% NH_3, 3.4% (NO + NH_3)	0.12, 1.0	MBMS	[20]

OH as well as temperature profiles in 38- and 78-Torr premixed hydrogen + air flames were obtained using laser-induced fluorescence (LIF). Though agreement of the experiments and the modeling with the GRI-mech. was imperfect, the NNH route was shown to be the major source of NO formation in these flames. These measurements were used by Konnov and De Ruyck [12] to prove that the rate constant of reaction of NNH oxidation by O atoms has a non-zero activation energy. Good agreement with the experiments was demonstrated using detailed H/N/O reaction mechanism [8].

Further experimental evidence for the NNH route of NO formation has been found by Hayhurst and Hutchinson [13] in rich ($\phi = 1.5$) $H_2 + O_2 + N_2$ flames at atmospheric pressure. They measured concentration profiles of NO in the flames with final temperature in the range 1850–2500 K and found that while Zeldovich mechanism explains the rate of NO production in the burnt gases of lean ($\phi = 0.75$) flames, the NNH route accounts, both qualitatively and quantitatively, for the accelerated NO formation in rich flames.

Flame seeding with nitrogen-containing compounds is used to study fuel–nitrogen conversion into NO_x or reburning of NO. For instance Morley [14] investigated the mechanism of formation of nitrogen oxides in rich $H_2 + O_2 + Ar$ flames ($\phi = 1.5$–2.6) doped with CH_3CN at atmospheric pressure. A calibration of NO fluorescence signal was obtained by adding NO alone to the flame. The NO signal was found to be constant through the burnt gas and proportional to the amount of NO added. Similar calibration procedure was used by Harrington et al. [10] and in many other flame studies by LIF. The rationale of this procedure is apparently based on the work of Cattolica et al. [15]. They used LIF for quantitative measurements of NO at the conditions of the experiments of Seery and Zabelski [16]. Seery and Zabelski [16] used molecular-beam mass-spectrometry (MBMS) for studying burner-stabilized $H_2 + O_2 + Ar$ flames at 76 Torr doped with 0.4–0.8% of NO over the range of equivalence ratios 0.88–1.74. It was shown that in the reaction zone (10 mm from the burner) NO concentration decreases by 25–35% in all flames. In the post-flame zone of lean flames the NO concentration rises to approximately the initial level, whereas in the rich flames further decrease of NO fraction by another 12–20% was observed. Cattolica et al. [15], however, did not confirm the findings of Seery and Zabelski [16]. Within the precision of the LIF measurements (±10%), no significant removal of nitric oxide was observed in these flames over the range of equivalence ratios 0.88–1.5.

Investigations of NO conversion at atmospheric pressure have been performed in rich ($\phi = 1.6$) [17] and in lean [18] premixed $H_2 + O_2 + Ar$ flames using probe sampling. Roby and Bowman [17] found that concentration of seeded NO (1750 ppm) rapidly decreases to about 60% of the initial value at about 1 mm above the burner surface, followed by a slower decay further downstream. Martin and Brown [18] studied, among others, lean ($\phi = 0.8$) $H_2 + O_2 + Ar$ flame doped with about 2100 ppm of NO. In the post-flame zone with the temperature of about 1600 K the destruction of NO did not exceed 8%.

NO reburning in $H_2 + O_2 + N_2$ flames at atmospheric pressure was only studied by Sepman et al. [19] using cavity ring-down absorption spectroscopy (CRDS) and LIF. The flame temperature was varied at fixed equivalence ratios ($\phi = 0.6$, 0.8, and 1.0) by changing the flow rate of the unburned mixture containing 200 ppm of NO. At the flame temperatures above ~1750 K, a good agreement (±5%) between the measured and seeded NO mole fraction was found. At the lower temperatures significant part of NO was consumed. The difference between the measured and seeded NO mole fractions reaches 30% at ~1450 K, which is substantially larger than the estimated experimental uncertainty. The authors pointed out that the modeling with the GRI-mech. [1] showed no loss of NO under these conditions and attributed NO removal to possible reactions on the burner surface. This explanation, if applicable to other experiments from the literature, may cast some doubts on the accuracy of the previous measurements and calls for detailed investigation of the flame structure of the $H_2 + O_2 + N_2$ flames seeded with NO at atmospheric pressure.

Ammonia conversion in premixed hydrogen flames was studied only in lean and stoichiometric mixtures diluted by argon [18,20,21]. Martin and Brown [18] found that at atmospheric pressure in lean flames ($\phi = 0.8$–0.86) doped with about 2000 ppm of NH_3 its conversion into NO depends on the flame temperature, which was varied by changing the flow rate of the unburned mixture. When the temperature was reduced from about 1600 K down to 1300 K the conversion ratio decreases from 63% to 43%. These results are consistent with the measurements of Di Julio and Knuth [21], who studied stoichiometric $H_2 + O_2 + Ar$ flame doped with 0.5% NH_3 at atmospheric pressure. In the post-flame zone (2 mm from the burner) at the flame temperature of ~1500 K, the conversion ratio of NH_3 to NO was found to be about 50%. Martin and Brown modeled and further analyzed their experimental results in [22]. Model predictions were found sensitive to the temperature profile (experimentally measured or calculated from energy equation), to the temperature of the flame holder and to the diffusion sub-model. It was also noticed that relatively little interconversion of nitrogen-containing species takes place at the heights above the burner greater than 1 mm.

At low pressure (34.5 Torr), lean ($\phi = 0.12$) and stoichiometric $H_2 + O_2 + Ar$ flames doped with ~3% of NO, or NH_3, or (NH_3 + NO) were studied using MBMS [20]. Final flame temperatures were rather moderate (1200–1450 K). No significant removal of NO seeded to these flames was noticed. In the stoichiometric flame, 3% of ammonia seeded produced about 1% of NO in the burnt gases, while in the very lean flame 3.4% NH_3 seeded produced about 1.8% of NO. Bian et al. [20] compared their measurements with the predictions of the Miller–Bowman mechanism [23] and found significant disagreement. They proposed several modifications to the rate constants of reactions of NH and NH_2 radicals,

which are important in the prediction of NO and N_2O concentration profiles.

One can conclude that experimental data on the flame structure of rich hydrogen flames doped with NH_3 at atmospheric pressure are still not available. Contradicting findings of Cattolica et al. [15] and of Seery and Zabelski [16] as well as unexpected behavior of NO reburning in $H_2 + O_2 + N_2$ flames [19] calls for detailed investigation of the flame structure of hydrogen flames seeded with NO at atmospheric pressure. The goal of the present work was, therefore, to study formation and consumption of NO in lean, near-stoichiometric and rich $H_2 + O_2 + N_2$ flames doped with 0.03–0.1% of NO or NH_3 using molecular-beam mass-spectrometry.

2. Experimental

The experimental setup for stabilizing flat flames has been described elsewhere [24], however, the most relevant details are repeated below. Premixed $H_2 + O_2 + N_2$ flames were stabilized on the burner shown in Fig. 1. The burner consisted of a tube 350 mm high with on its top a copper plate 24 mm in diameter and 3 mm thick, perforated with 0.5-mm diameter holes spaced uniformly with a pitch of 0.7 mm. This drilling pattern is similar to those used in other flame studies using the Heat Flux method, e.g. [2,4,9,25–27]. The copper plate and fresh gas mixture were heated using circulating water and two thermostats. The temperature of the plate edges was maintained at 60 °C and the temperature of the fresh mixture consisting of hydrogen, oxygen and nitrogen at 35 °C. These temperatures were chosen the same as in the previous studies, e.g. [24,28]. Compositions and flow rates of the fresh mixtures were set by mass flow controllers (MKS Instruments). The radial temperature distribution on the burner surface was measured by copper–constantan thermocouples, the junctions of which were soldered into the burner holes at the distances of 0, 2.4, 4.5, 7, 10, and 12 mm from the center of the burner.

$H_2 + O_2 + N_2$ flames of three different compositions were stabilized on the burner described above. Dilution ratios $D = [O_2]/([O_2] + [N_2])$ for the flames with $\phi = 0.47$, 1.1 and 2.0 were 0.209, 0.09, and 0.077, respectively. The characteristics of the flames studied are presented in Table 2. The choice of these flames was defined by several reasons. On the one hand, the dilution ratio was chosen in such a way as to have low post-flame temperature in order to prevent formation of NO from N_2 via thermal Zeldovich mechanism. On the other hand, selecting low-temperature flames

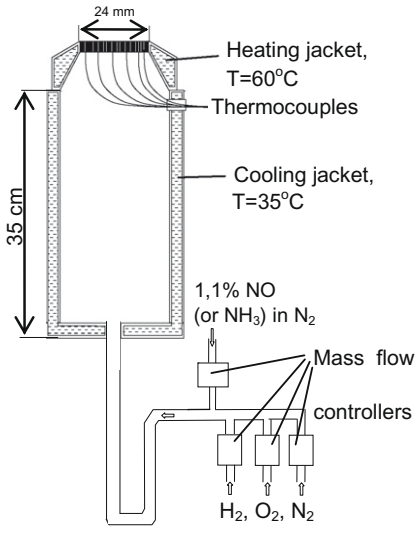

Fig. 1. Schematic of the Heat Flux burner.

Table 2
Characteristics of the studied flames.

Flame	$H_2 + O_2 + N_2$		
Equivalence ratio	0.47	1.1	2.0
$D = [O_2]/([O_2] + [N_2])$	0.209	0.09	0.077
NO or NH_3 addition (ppm)	1000, 300	1000, 300	1000, 300
Measured flame speed (cm/s)	55	47	41.1
Calculated burning velocity (cm/s)	36.2	38.3	39.6
Gas velocity in experiment (cm/s)	34.24	42.5	40.7
Measured temperature in the post-flame zone (K)	1443	1366	1193

prevented fusion of quartz probes, which are used for studying the flame structure, and provided a fairly wide reaction zone of the flames in order to improve the accuracy of the spatial resolution of the sampling probe. Dilution ratios and equivalence ratios were chosen the same as in the previous studies [24,29].

The velocities of unburnt gases for the flames with $\phi = 1.1$ and 2.0 were chosen 1–5 cm/s less than the burning velocities of the flames measured using the Heat Flux method on the burner described above. This method [26,27] is based on balancing of the heat loss required for flame stabilization by the convective heat flux from the burner surface to the flame front. The lean flame ($\phi = 0.47$) under the near-adiabatic conditions (according to the measurements using the Heat Flux method) was found to have cellular structure. Doping a trace amount of hydrocarbons (e.g. hexane or octane) into the fresh mixture in special tests clearly revealed the cellular structure of the lean flame. To make the flame laminar, the velocity of unburnt gases was kept 40% less than the speed of the cellular flame, and only 2 cm/s lower than the calculated burning velocity. The measured and simulated flame speeds as well as the flow velocities of the fresh mixtures specified in the experiments are listed in Table 2. The purity of H_2, O_2, and N_2 was 99.95%. NO and NH_3 were added to the unburnt gases as 1.10% mixtures with pure N_2 (99.999%).

The concentration profiles of the combustion products were measured using quadrupole mass spectrometer MS7302 coupled with molecular-beam sampling system [30]. The mass spectrometer was equipped with improved ion source with a narrow spread of electron energies (±0.25 eV), which corresponds to the thermal scattering of electron energy (approximately 2 kT, where k is Boltzmann constant and T is cathode temperature) [31]. This allowed operating at low ionization energies, which are close to the ionization potentials of the atoms, radicals and molecules. Data acquisition system is described in details elsewhere [31]. The mass peaks corresponding to stable flame species (H_2, O_2, H_2O, NO) were measured at ionization energy of electrons of 18 eV, the 17 AMU peak (NH_3) was measured at 12.5 eV, the peaks of 1 and 17 AMU (H and OH) were measured at 16.2 eV. Sampling was performed using a quartz probe with the orifice diameter of 0.08 mm and inner angle of 40°.

Calibration coefficients for the stable species were determined by direct calibration using the mixtures of known composition. Calibration of H and OH radicals was performed using a method proposed earlier [32]. This method is based on the consideration that in the post-flame zone of hydrogen flames partial equilibrium of three "fast" reactions

$$H_2 + OH = H_2O + H \quad (1)$$

$$H_2 + O = H + OH \quad (2)$$

$$O_2 + H = OH + O \quad (3)$$

takes place. The concentrations of H, O and OH in this approximation can be expressed using equilibrium constants of reactions (1)–(3), concentrations of the stable species (H_2, O_2, and H_2O) and

temperature. Direct implementation of this approach in all flames with ϕ = 0.47, 1.1 and 2.0 studied in the present work was, however, not possible. This is because of the relatively low post-flame temperature (1200–1350 K), which hinder attaining of the partial equilibrium. It was also confirmed by comparison of the concentrations of H and OH calculated in assumption of the partial equilibrium using equations presented elsewhere [24] with detailed flame structure modeling using Premix code and detailed kinetic mechanism [8]. For this reason a hotter flame (calibration flame) with the post-flame temperature of 1600 K was used for calibration. Absolute concentrations of H and OH in the post-flame zone (at 1.2–1.5 mm) of the calibration flame (ϕ = 1.1, D = 0.14) have been determined. The calibration coefficients of H and OH were assumed the same in all flames studied (lean, near-stoichiometric and rich). Details of this method were described by the authors earlier [24].

To ensure correct and reproducible data, each cycle of concentration measurements at every spatial point was repeated three times and mean-square errors were determined. In our experiments, uncertainties of the intensities of the measured peaks varied from 5–10% for 2 AMU (H_2) and 32 AMU (O_2) to 10–30% for 1 AMU (H) and 17 AMU (OH). Typically, the uncertainty of the measurements for 30 AMU (NO) and 17 AMU (NH3) was 5–15%. Uncertainties associated with the concentration measurements are shown in subsequent figures as error bars. In some cases they much exceeded typical uncertainties mentioned above due to very low concentrations approaching detection limits. Gas-dynamic perturbations of the flame by a probe were taken into account by shifting the obtained profiles upstream by the distance ΔZ evaluated as $\Delta Z = 0.37 \cdot d \cdot \sqrt{\frac{Q}{S \cdot V}}$, where d is diameter of the orifice, Q is volumetric flow rate though the orifice, S is area of the orifice and V is velocity of the flow riding onto the probe [33]. Maximal value of the shift corresponds to position of the probe near the burner and does not exceed 0.3 mm.

Temperature profiles were measured using Pt/Pt + 10%Rh thermocouple made of wires 0.02 mm in diameter and coated with SiO_2; total diameter of the coated thermocouple was ~0.04 mm. The thermocouple junction was placed at the distance 0.15–0.2 mm from the probe's orifice. To validate this choice, temperature profiles in the near-stoichiometric flame with the thermocouple positioned at different distances from the probe tip (0.1, 0.2, 0.3 and 0.4 mm) were measured. Calculated flame structure using these profiles and detailed kinetic mechanism [8] was then compared with the measurements. The best match of the calculated and experimental maximums of H and OH concentration profiles was found for the temperature profile obtained at the distance "probe tip – thermocouple junction" somewhere between 0.15 and 0.2 mm. Since the conditions (post-flame temperature, velocity of the flow riding onto the probe) for lean (ϕ = 0.47) and rich (ϕ = 2.0) $H_2 + O_2 + N_2$ flames studied are similar to those for near-stoichiometric flame (ϕ = 1.1), the appropriate position of the thermocouple relative to the probe tip was assumed to be the same. The temperature was measured with an accuracy of ±25 K, the radiative heat losses of the thermocouple were taken into account. Correction due to radiation was typically about $\leqslant$50 K and was determined as described elsewhere [34].

3. Modeling details

The flame structure was simulated using Premix code from the Chemkin-II collection of codes and extensively validated H/N/O mechanism [8]. This mechanism is an integral part of the Konnov detailed reaction mechanism for small hydrocarbons combustion [3]. Experimentally measured temperature profiles were used as input data for the modeling. Windward differencing was used and the grid was refined according to adaptive mesh parameters GRAD = 0.02 and CURV = 0.5; multi-component and thermal diffusion options were used in the calculations.

4. Results and discussion

4.1. Neat hydrogen flames

Figs. 2–4 show measured and simulated profiles of concentration of the stable species, H_2, O_2 and H_2O, in lean (ϕ = 0.47, D = 0.209), near-stoichiometric (ϕ = 1.1, D = 0.09) and rich (ϕ = 2.0, D = 0.077) flames, respectively. Error bars in these and subsequent figures represent experimental uncertainties. Moderate disagreement between the measured and simulated concentrations of H_2O is observed near the burner surface. This disagreement is caused by the variation of H_2O calibration coefficient with the flame temperature. It occurs due to formation of water clusters

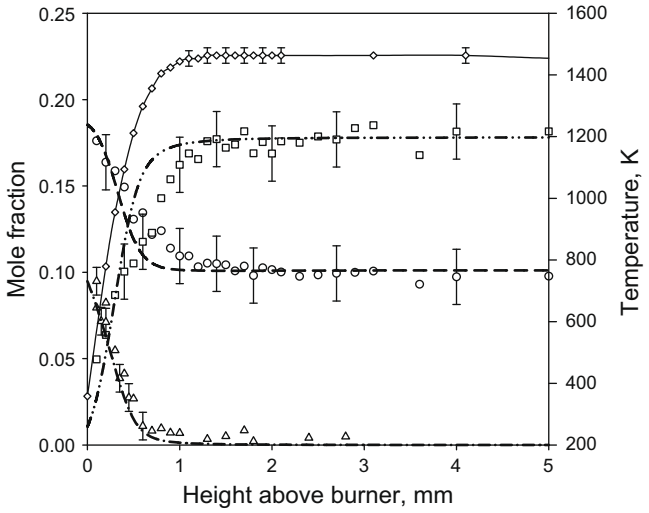

Fig. 2. Profiles of temperature and concentration of H_2, O_2 and H_2O in the lean flame. Lines are modeling, symbols are measurements. Diamonds and solid line: temperature, triangles and dash–dot line: H_2, circles and dashed line: O_2, squares and dash–double dot line: H_2O.

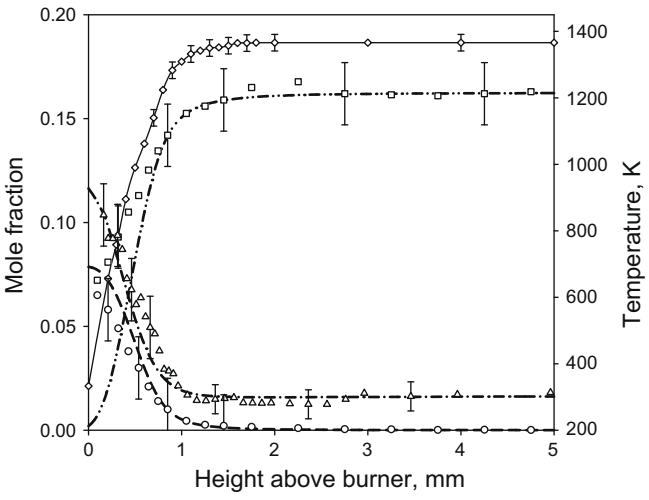

Fig. 3. Profiles of temperature and concentration of H_2, O_2 and H_2O in the near-stoichiometric flame. Lines are modeling, symbols are measurements. Diamonds and solid line: temperature, triangles and dash–dot line: H_2, circles and dashed line: O_2, squares and dash–double dot line: H_2O.

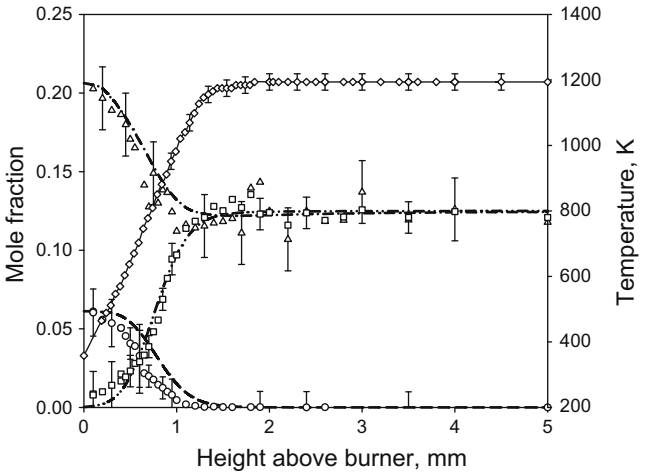

Fig. 4. Profiles of temperature and concentration of H_2, O_2 and H_2O in the rich flame. Lines are modeling, symbols are measurements. Diamonds and solid line: temperature, triangles and dash–dot line: H_2, circles and dashed line: O_2, squares and dash–double dot line: H_2O.

in the nozzle of the probe when sampling in the low-temperature zone of the flame. This effect was experimentally observed during calibration by $N_2 + H_2O$ gas mixture, which was delivered to the probe through a tubular heater. Thus, the measured concentrations of H_2O at temperatures lower than ~500 K are over-estimated. The characteristic width of the reaction zone both in the measurements and modeling is about 1 mm for all flames studied.

Figs. 5–7 show measured and simulated spatial profiles of H and OH concentration in lean ($\phi = 0.47$, $D = 0.209$), near-stoichiometric ($\phi = 1.1$, $D = 0.09$) and rich ($\phi = 2.0$, $D = 0.077$) flames, respectively. Due to low concentration of H in the lean flame and of OH in the rich flame, the profiles of these species were measured with insufficient accuracy and they are not presented in these figures. Concentration of H and OH in the lean and near-stoichiometric flames reaches its maximum at 1 mm from the burner and in the rich flame at about 1.5 mm. However, the maximums of the simulated H and OH concentration profiles are observed 0.1–0.3 mm closer to the burner than those obtained in the experiment. Also the calculated profiles are somewhat steeper than the experimental ones, especially in the reaction zone of all flames. There are two apparent reasons for this discrepancy. First, the spatial resolution of the probe with the orifice diameter of 0.08 mm is typically

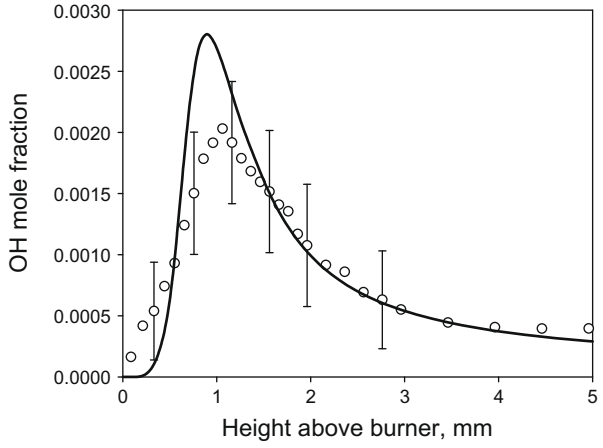

Fig. 5. Profiles of OH concentration in the lean flame. Line is modeling, symbols are measurements.

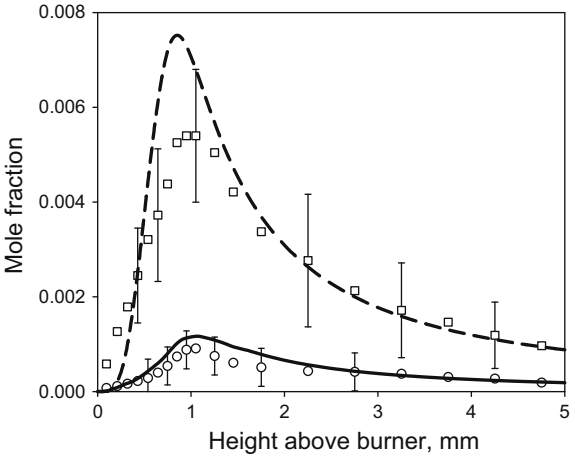

Fig. 6. Profiles of OH and H concentration in the near-stoichiometric flame. Lines are modeling, symbols are measurements. Circles and solid line: OH, squares and dashed line: H.

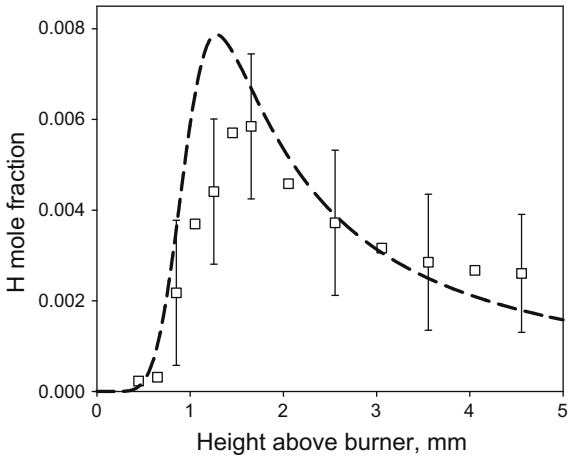

Fig. 7. Profile of H concentration in the rich flame. Line is modeling, symbols are measurements.

0.1–0.2 mm [33,35]. Consequently, the concentrations measured by the probe are spatially averaged values; thus, the steep gradients cannot be accurately resolved, and the peak values are somewhat lower. Second, the choice of the optimal distance "probe tip – thermocouple junction", at which the temperature profile was measured and then used in the modeling, was made in the near-stoichiometric flame as described above. Discrepancy of the position of the calculated and experimental maximums of radical concentration mostly visible in rich flame (Fig. 7) indicates that assumption of the similar thermal structure of the flames is not completely valid. Much better agreement could be achieved using individually adjusted temperature profiles for the flames of different stoichiometry. However, this approach could introduce additional ambiguity in the analysis and comparison of different flames, and therefore was not implemented in the present work.

4.2. Flames doped with NO

Flame doping with NO did not affect concentration profiles of the stable species, H_2, O_2 and H_2O, within the experimental uncertainty. Figs. 8–10 present measured and simulated spatial profiles of NO concentration in NO-doped (300 and 1000 ppm) lean ($\phi = 0.47$, $D = 0.209$), near-stoichiometric ($\phi = 1.1$, $D = 0.09$) and rich

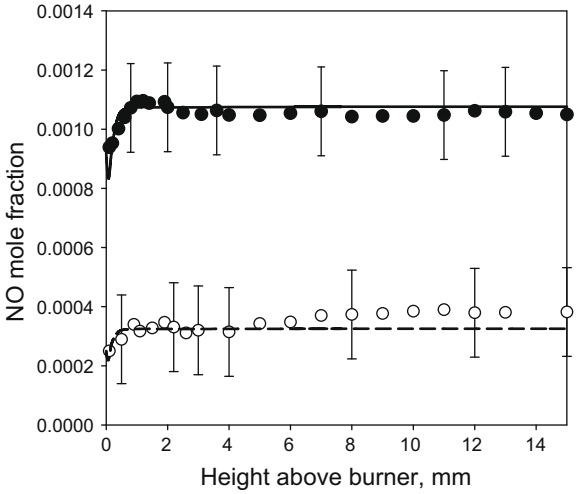

Fig. 8. Profiles of NO concentration in the lean flames doped with 300 and 1000 ppm of NO. Lines are modeling using original [8] and modified mechanisms, symbols are measurements. Black symbols and solid line: flame doped with 1000 ppm of NO, open symbols and dashed line: flame doped with 300 ppm of NO.

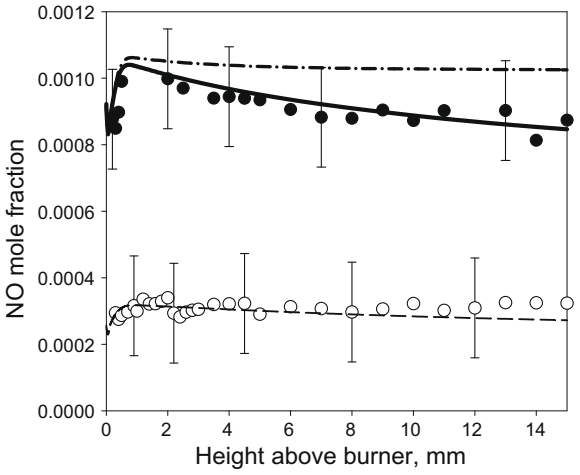

Fig. 9. Profiles of NO concentration in the near-stoichiometric flames doped with 300 and 1000 ppm of NO. Lines are modeling, symbols are measurements. Black symbols, solid and dash–dot lines: flame doped with 1000 ppm of NO, open symbols and dashed line: flame doped with 300 ppm of NO. Solid line: modeling using the original mechanism [8], dash–dot line: modeling using modified mechanism.

(ϕ = 2.0, D = 0.077) flames, respectively. In the lean flame small initial rise of [NO] in the flame front is followed by plateau; the concentration of NO in the post-flame zone is very close to the amount doped into the fresh mixture. In the near-stoichiometric and rich flames nitric oxide doped into the fresh mixture is gradually consumed in the post-flame zone. This consumption is most notable at the high load of NO (1000 ppm). Narrow zone of NO consumption and following formation is clearly observed near the burner in the reaction zone of the rich flames. It occurs due to oxidation of NO into NO_2, which in turn decomposes back to NO at higher temperatures in the flame front. An overall conversion ratio of NO defined as $C_{NO} = ([NO]_0 - [NO]_{fin})/[NO]_0$, where $[NO]_0$ is initial concentration and $[NO]_{fin}$ is the concentration at 12–15 mm from the burner, varies from 0 to 0.1 with the tendency of modest increase as ϕ and/or doped amount of NO rise.

Predictions of the original mechanism [8] are also shown in Figs. 8–10 as solid lines for 1000 ppm of NO doped and dashed

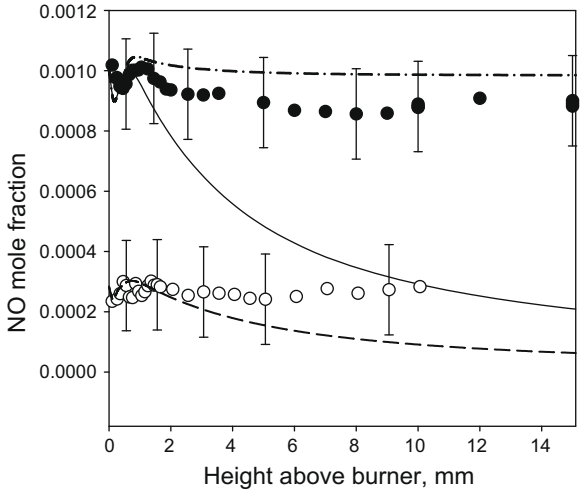

Fig. 10. Profiles of NO concentration in the rich flames doped with 300 and 1000 ppm of NO. Black symbols, solid and dash–dot lines: flame doped with 1000 ppm of NO, open symbols and dashed line: flame doped with 300 ppm of NO. Solid line: modeling using the original mechanism [8], dash–dot line: modeling using modified mechanism.

lines for 300 ppm of NO doped. Agreement of the modeling and measurements is remarkably good in the lean and near-stoichiometric flames. However, in the rich flames, the model predicts NO conversion ratio to be 0.75–0.8, whereas the measured value is not higher than 0.1. To reveal the reasons of the disagreement between the measurements and modeling, the integral analysis of consumption rates of NO through all pathways was made. To analyze the reaction pathways of nitric oxide transformation in flames, an investigation of N-element fluxes from species to species was performed using the Kinalc code [36], a post-processor of the output files of the Premix code. Since the element flux analysis should be carried out with a reaction mechanism containing irreversible reactions only, the original mechanism [8] was first converted into the irreversible form by the Mechmod code [37]. The Flux Viewer code [38] was used to visualize N-fluxes. Fig. 11 shows the reaction pathways of NO transformation at the distance of 6 mm above the burner in the rich $H_2 + O_2 + N_2$ flame doped with 1000 ppm of NO. The key pathways of NO consumption were found to be the stages involving N and H:

$$NO + N => N_2 + O \quad (4)$$

$$H + NO(+M) => HNO(+M) \quad (5)$$

According to the reaction mechanism [8], HNO formed in reaction (5) reacts further with H_2:

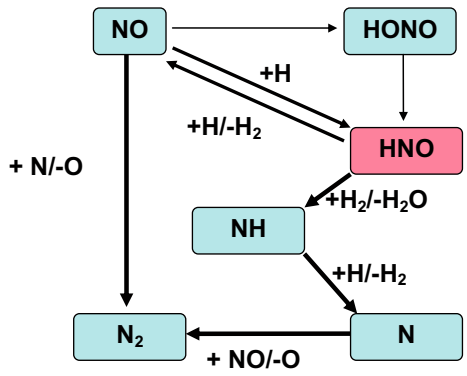

Fig. 11. Reaction pathways of NO transformation at the distance of 6 mm above the burner in the rich flame doped with 1000 ppm of NO.

$$HNO + H_2 => NH + H_2O \quad (6)$$

Since H_2 concentration in the post-flame zone of the rich flame is quite high (12% by volume), the calculated consumption rate of NO is much higher under rich conditions. Thus, the key stages, responsible for NO consumption in rich flames, are the reactions of HNO. Reaction pathway analysis performed using the GRI-mech. 3.0 [1] brought up the same results in the rich $H_2 + O_2 + N_2$ flame.

These findings were supported by the results of sensitivity analysis also performed for the irreversible mechanism. The sensitivity coefficients of NO concentration with respect to reaction rates are shown in Fig. 12. The key stages of NO conversion in the post-flame zone of the rich flame are reaction (5) and

$$HNO + H => NO + H_2 \quad (7)$$

$$NH + H_2O => HNO + H_2 \quad (8)$$

In the post-flame zone of the lean and stoichiometric flames these reactions play minor role. Modifications of the rate constants of reactions (6)–(8) therefore could improve agreement of the modeling with experiment in the rich flames without significant deterioration in the lean and stoichiometric flames.

From the reactions considered the only good candidate for the modification is reaction (6), which is reverse of reaction (8). Reaction (8) has been implemented in the original mechanism [8] (as well as in the GRI-mech. 3.0 [1]) with the rate constant measured by Rohrig and Wagner [39] and with HNO and H_2 as assumed products based on thermodynamic consideration. Since then analysis of the nitric oxide reburning in a flow reactor [40] and in a jet-stirred reactor [41] clearly ruled out a significant conversion of HNO to NH through reaction (6). Therefore Glarborg et al. [40] and Dagaut et al. [41] concluded that reversible reaction

$$NH + H_2O = HNO + H_2 \quad (8rev)$$

is slow and removed it from their models. Further quantum chemical and experimental studies [42,43] strongly supported the measurements of Rohrig and Wagner [39] for direct reactions between NH and H_2, H_2O, and CO_2 rejecting, however, HNO and H_2 as the products of reaction (8).

In fact Rohrig and Wagner [39] proposed also NH_2OH or H_3NO as possible products of the reaction between NH and H_2O. Therefore reaction

$$NH + H_2O = HNO + H_2 \quad (8rev)$$

was replaced by reversible reaction

$$NH + H_2O = NH_2OH \quad (8new)$$

with the same rate constant. This replacement has no effect in the lean flames, little effect in the stoichiometric flames, and significantly improves agreement of the modified mechanism with the experiments in the rich flames. These modeling results are shown in Figs. 9 and 10 by dash–dot lines. This is the only modification to the original mechanism [8] required for accurate predictions of nitric oxide concentrations in $H_2 + O_2 + N_2$ flames doped with NO.

4.3. Flames doped with NH_3

Flame doping with NH_3 did not affect concentration profiles of the stable species, H_2, O_2 and H_2O, within the experimental uncertainty. Figs. 13–15 present measured and simulated profiles of NH_3 concentration in NH_3-doped (300 and 1000 ppm) lean (ϕ = 0.47, D = 0.209), near-stoichiometric (ϕ = 1.1, D = 0.09) and rich (ϕ = 2.0, D = 0.077) flames, respectively. The zone of NH_3 consump-

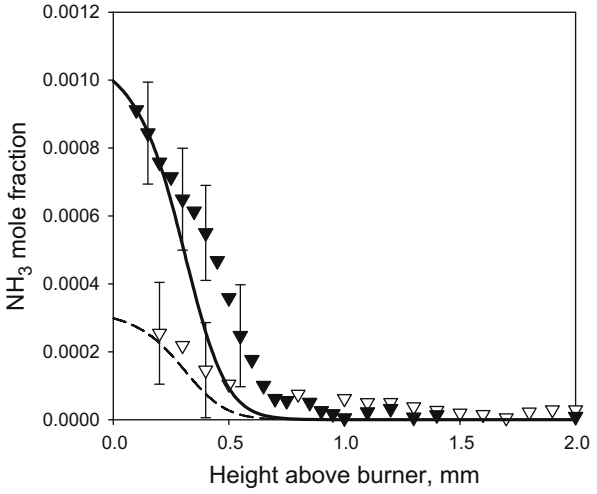

Fig. 13. Concentration profiles of NH_3 in the lean flames doped with 1000 and 300 ppm of NH_3. Lines are modeling, symbols are experiment. Solid line and black symbols are for 1000 ppm of NH_3, dashed line and open symbols are for 300 ppm of NH_3.

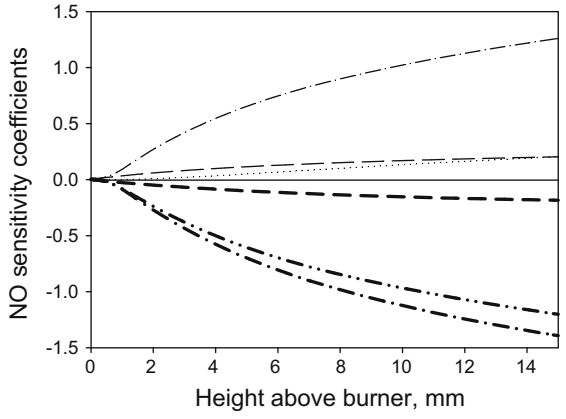

Fig. 12. Sensitivity coefficients of NO concentration in flames doped with 1000 ppm of NO. Thin dash and dot line: reaction (7) HNO + H => NO + H_2 (ϕ = 2.0); thin dashed line: (7) HNO + H => NO + H_2 (ϕ = 1.1); thin coinciding solid lines: (7) HNO + H => NO + H_2 (ϕ = 0.47), (5) H + NO(+M) => HNO(+M) (ϕ = 0.47); thin dotted line: (8) NH + H_2O => HNO + H_2 (ϕ = 2.0); thick dashed line: (5) H + NO(+M) => HNO(+M) (ϕ = 1.1); thick dash and dot line: (5) H + NO(+M) => HNO(+M) (ϕ = 2.0); thick dash and double dot line: (6) HNO + H_2 => NH + H_2O (ϕ = 2.0).

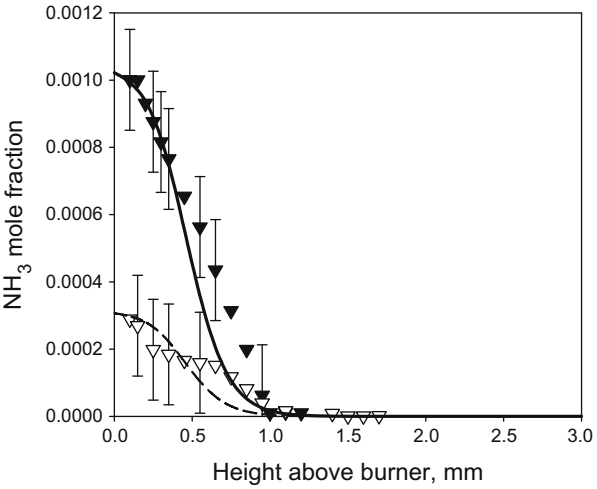

Fig. 14. Concentration profiles of NH_3 in the near-stoichiometric flames doped with 1000 and 300 ppm of NH_3. Lines are modeling, symbols are experiment. Solid line and black symbols are for 1000 ppm of NH_3, dashed line and open symbols are for 300 ppm of NH_3.

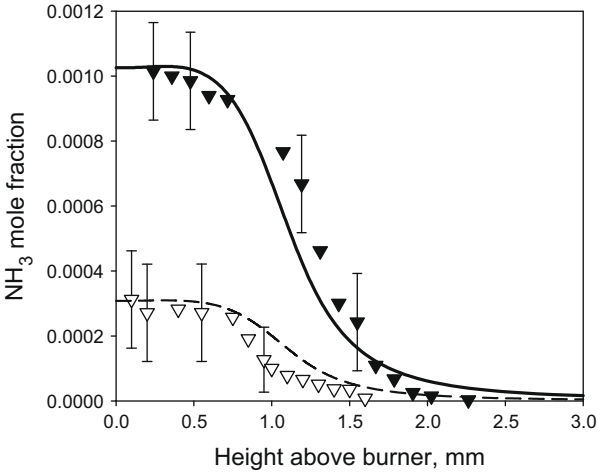

Fig. 15. Concentration profiles of NH_3 in the rich flames doped with 1000 and 300 ppm NH_3. Lines are modeling, symbols are experiment. Solid line and black symbols are for 1000 ppm of NH_3, dashed line and open symbols are for 300 ppm of NH_3.

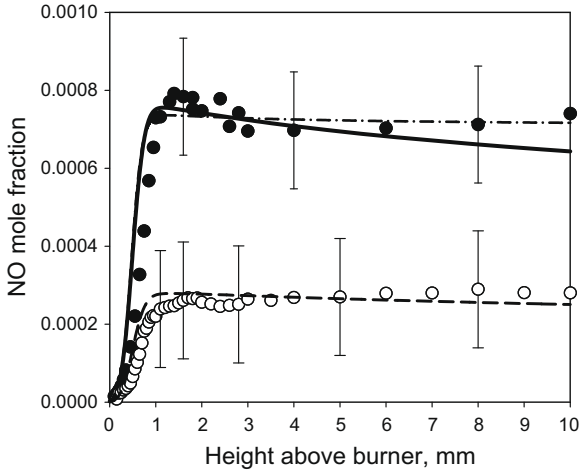

Fig. 17. Concentration profiles of NO in the near-stoichiometric flames doped with 300 and 1000 ppm of NH_3. Lines are modeling, symbols are experiment. Solid, dash–dotted lines and black symbols are for 1000 ppm of NH_3, dashed line and open symbols are for 300 ppm of NH_3. Solid and dashed lines correspond to the original mechanism [8]; thin dash–dotted line corresponds to modified mechanism (case 2).

tion is about 0.6–0.8 mm in the lean and near-stoichiometric flames and is about 1.7–1.9 mm in the rich one. Predictions of the original mechanism [8] are also shown in Figs. 13–15 as solid lines for 1000 ppm of NH_3 doped and as dashed lines for 300 ppm of NH_3 doped. Agreement of the modeling and measurements is good in all flames.

Figs. 16–18 present measured and simulated spatial profiles of NO concentration in NH_3-doped (300 and 1000 ppm) lean, near-stoichiometric and rich flames, respectively. Predictions of the original mechanism [8] are also shown in Figs. 16–18 as solid lines for 1000 ppm of NH_3 doped and as dashed lines for 300 ppm of NH_3 doped. In these flames, an overall conversion ratio of NH_3 into NO defined as $C_{NH3} = [NO]_{fin}/[NH_3]_0$, where $[NH_3]_0$ is initial concentration of ammonia and $[NO]_{fin}$ is the concentration of NO at 5–6 mm from the burner, reduces from 1 to 0.12–0.15 as equivalence ratio rises from 0.47 to 2.0. In the lean and near-stoichiometric flames, NO concentration practically does not change from 2 to 10 mm above the burner. This observation is probably applicable to the rich flames as well. One should note that due to much lower concentrations of NO in the rich flames, relative experimental uncertainty is much higher, Fig. 18. In this Figure odd error bars correspond to 1000 ppm of NH_3 doped and even ones to 300 ppm of NH_3 doped.

Model predictions are in good quantitative agreement with the measured concentrations of NO in all flames within the experimental uncertainty. However, qualitative trends observed in the rich flames are of concern. Particularly, the calculated concentrations of NO in the burnt gases of the flames doped with 300 or 1000 ppm of NH_3 are almost the same, while the measured concentrations are different by a factor of ~3. Since the relative values of NO concentration do not include calibration uncertainty, this qualitative disagreement may indicate some deficiencies in the kinetic mechanism.

To look for possible modifications to the model, sensitivity and reaction path analyses similar to those implemented for the flames

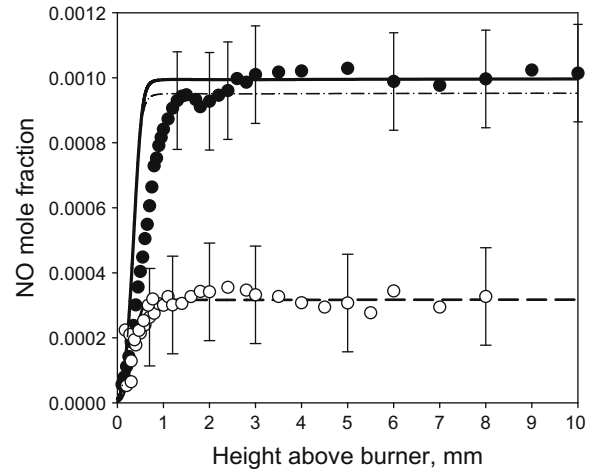

Fig. 16. Concentration profiles of NO in the lean flames doped with 300 and 1000 ppm of NH_3. Lines are modeling, symbols are experiment. Solid, dotted lines and black symbols are for 1000 ppm of NH_3, dashed line and open symbols are for 300 ppm of NH_3. Solid and dashed lines correspond to the original mechanism [8]; thin dash–dotted line corresponds to modified mechanism (case 2).

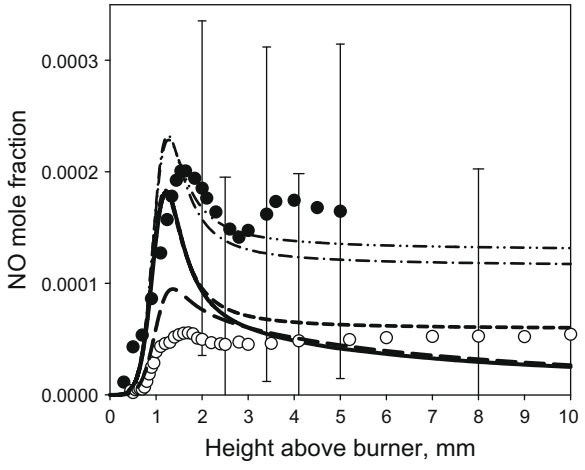

Fig. 18. Concentration profiles of NO in the rich flames doped with 300 and 1000 ppm of NH_3. Lines are modeling, symbols are experiment. Solid, short–dashed, dash–dotted, dash–double dotted lines and black symbols are for 1000 ppm of NH_3, long-dashed line and open symbols are for 300 ppm of NH_3. Solid and dashed lines correspond to the original mechanism [8]; short–dashed line corresponds to the mechanism with reaction (8rev) replaced by reaction (8new); thin dash–dotted line corresponds to modified mechanism (case 1); thin dash–double dotted line corresponds to modified mechanism (case 2).

doped with NO have been performed. Fig. 19 shows reaction pathways of ammonia consumption at the distance of 6 mm from the burner in the rich flame doped with 1000 ppm of NH_3. This analysis has been performed with the irreversible original mechanism [8]. The main stages of NH_3, NH_2 and NH consumption are reactions with H atoms:

$$NH_3 + H => NH_2 + H_2 \quad (9)$$

$$NH_2 + H => NH + H_2 \quad (10)$$

$$NH + H => N + H_2 \quad (11)$$

Then, N atoms are consumed either in reaction with OH:

$$N + OH => NO + H \quad (12)$$

or in reaction with NO:

$$NO + N => N_2 + O \quad (4)$$

resulting N_2. Thus, the balance between reactions (12) and (4) defines the rate of NO formation and destruction in the post-flame zone of the rich NH_3-doped flame. Part of NH radicals are oxidized in reaction

$$NH + H_2O => HNO + H_2 \quad (8)$$

forming HNO. However, contrary to the pathways of HNO transformation in the NO-doped flames (Fig. 11), reverse reaction

$$HNO + H_2 => NH + H_2O \quad (6)$$

is not very important in the NH_3-doped flame. Replacement of reaction

$$NH + H_2O = HNO + H_2 \quad (8rev)$$

by reversible reaction

$$NH + H_2O = NH_2OH \quad (8new)$$

only slightly improves the agreement of the modeling with the measured concentrations of NO. The calculated concentration profile of NO in this case is shown in Fig. 18 as short-dash line.

Sensitivity analysis of NO formation with respect to reaction rate constants has been performed for the lean, near-stoichiometric and rich flames doped with 1000 ppm of NH_3. The sensitivity coefficients defined in the rich flame are shown in Fig. 20. Key steps controlling NO consumption in the NO-doped rich flame, reactions (6) and (8), are also presented in Fig. 20, but their sensitivity is less in the NH_3-doped flame than in the NO-doped one. The most sensitive are reactions (12) and (4) in agreement with the reaction path analysis. The rate constants of these reactions in the present mechanism [8] were adopted from the review [44], where logarithmic uncertainty of the rate constant of reaction (12) was evaluated as $\Delta \log k = \pm 0.3$–0.4, while for reaction (4) as $\Delta \log k = \pm 0.15$. Independent modifications of these rate constants required for good matching of the concentration profile of NO in the rich NH_3-doped flame are too high and are at the limit of their uncertainty. To illustrate these modifications two modeling cases were attempted: in the case 1 pre-exponential factor of the rate constant of reaction $N_2 + O = NO + N$ was decreased from 1.8×10^{14} to 1.1×10^{14} and reaction (8rev) was replaced by reaction (8new); in the case 2 pre-exponential factor of the rate constant of reaction (12) was increased from 2.8×10^{13} to 6.2×10^{13} and reaction (8rev) was replaced by reaction (8new). The simulated profiles of NO concentration using the both cases are shown in Figs. 16–18. Each of the above changes resulted in a visually improved agreement between the experimental and modeling results especially in the rich flame doped with 1000 ppm of NH_3.

These independent modifications, however, are not justified and not implemented in the present mechanism. Indeed, Morley [14] and Haynes [45] demonstrated that the ratio of the rate constants of reactions (12) and (4) is essentially constant and close to unity at the temperatures typical for post-flame zones of hydrogen and hydrocarbon flames. Thus the range of allowable modifications is even smaller than the logarithmic uncertainty of the rate constant of reaction (4). Clearly more accurate measurements of NO in rich hydrogen flames doped with NH_3 are required to prove or reject the need for further model adjustment.

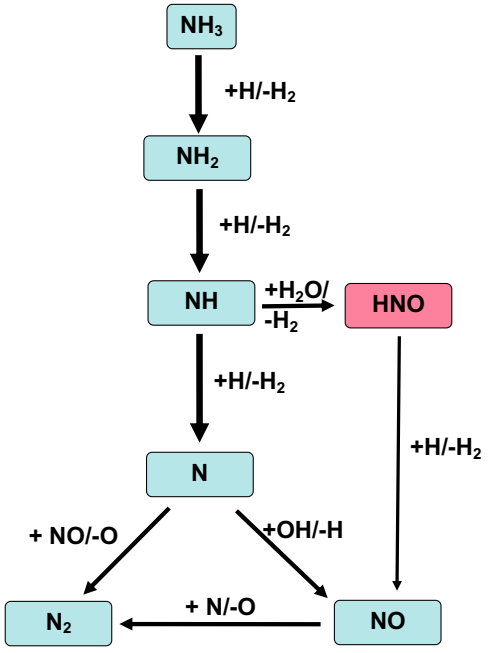

Fig. 19. Reaction pathways of NH_3 transformation in the rich flame doped with 1000 ppm of NH_3 at the distance of 6 mm above the burner.

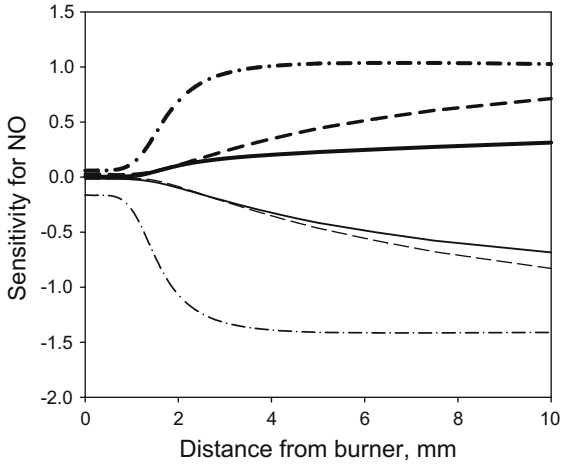

Fig. 20. Sensitivity coefficients of NO concentration in the rich flame doped with 1000 ppm of NH_3. Thick solid line: reaction (8) $NH + H_2O => HNO + H_2$; thick dashed line: (7) $HNO + H => NO + H_2$; thick dash and dot line: (12) $N + OH => NO + H$; thin solid line: (6) $HNO + H_2 => NH + H_2O$; thin dashed line: (5) $H + NO(+M) => HNO(+M)$; thin dash and dot line: (4) $NO + N => N_2 + O$.

5. Conclusions

New experimental data on the structure of $H_2 + O_2 + N_2$ flames of various compositions doped with 300 and 1000 ppm of NO or NH_3 provide extended basis for model validation. Comparison of the modeling and experiments revealed a necessity of refining the mechanism developed earlier to predict the structure of the

rich $H_2 + O_2 + N_2$ flames. The analysis of reaction pathways and the sensitivity analysis allowed to identify the reactions responsible for the disagreement between experiment and modeling. A modified mechanism, in which reaction

$$NH + H_2O = HNO + H_2 \quad (8rev)$$

was replaced by reversible reaction

$$NH + H_2O = NH_2OH \quad (8new)$$

provided a good agreement between the experimental and modeling data on spatial profiles of NO and NH_3 concentration in the lean ($\phi = 0.47$), near-stoichiometric ($\phi = 1.1$) and rich ($\phi = 2.0$) $H_2 + O_2 + N_2$ flames doped with either NO or NH_3.

Acknowledgments

The Russian Foundation of Basic Research is acknowledged for the support of this work through Grant No. 05-03-34815-MF-a.

References

[1] G.P. Smith, D.M. Golden, M. Frenklach, N.W. Moriarty, B. Eiteneer, M. Goldenberg, C.T. Bowman, R.K. Hanson, S. Song, W.C. Gardiner Jr., V.V. Lissianski, Z. Qin, GRI-Mech 3.0, 1999. <http://www.me.berkeley.edu/gri_mech/>.
[2] D.A. Knyazkov, A.G. Shmakov, I.V. Dyakov, O.P. Korobeinichev, J. De Ruyck, A.A. Konnov, Proc. Combust. Inst. 32 (2009) 327–334.
[3] A.A. Konnov, Detailed reaction mechanism for small hydrocarbons combustion. Release 0.5, 2000, available as Electronic Supplementary Material to [25].
[4] A.A. Konnov, I.V. Dyakov, J. De Ruyck, Combust. Sci. Technol. 178 (2006) 1143–1164.
[5] O. Skreiberg, P. Kilpinen, P. Glarborg, Combust. Flame 136 (2004) 501–518.
[6] J.B. Homer, M.M. Sutton, Combust. Flame 20 (1973) 71–76.
[7] A.A. Konnov, Combust. Flame 134 (2003) 421–424.
[8] A.A. Konnov, J. De Ruyck, Combust. Sci. Technol. 168 (2001) 1–46.
[9] A.A. Konnov, I.V. Dyakov, J. De Ruyck, Proc. Combust. Inst. 29 (2002) 2171–2177.
[10] J.E. Harrington, G.P. Smith, P.A. Berg, A.R. Noble, J.B. Jeffries, D.R. Crosley, Proc. Combust. Inst. 26 (1996) 2133–2138.
[11] J.W. Bozzelli, A.M. Dean, Int. J. Chem. Kinet. 27 (1995) 1097.
[12] A.A. Konnov, J. De Ruyck, Combust. Flame 125 (2001) 1258–1264.
[13] A.N. Hayhurst, E.M. Hutchinson, Combust. Flame 114 (1998) 274–279.
[14] C. Morley, Proc. Combust. Inst. 18 (1981) 23–31.
[15] R.J. Cattolica, J.A. Cavolowsky, T.G. Mataga, Proc. Combust. Inst. 22 (1988) 1165–1173.
[16] D.J. Seery, M.F. Zabielski, Proc. Combust. Inst. 18 (1981) 397–403.
[17] R.J. Roby, C.T. Bowman, Combust. Flame 70 (1987) 119–123.
[18] R.J. Martin, N.J. Brown, Combust. Flame 80 (1990) 238–255.
[19] A.V. Sepman, V.M. van Essen, A.V. Mokhov, H.B. Levinsky, Appl. Phys. B 77 (2003) 109–117.
[20] J. Bian, J. Vandooren, P.J. Van Tiggelen, Proc. Combust. Inst. 23 (1990) 379–386.
[21] S.S. Di Julio, E.L. Knuth, Combust. Sci. Technol. 66 (1–3) (1989) 149–155.
[22] R.J. Martin, N.J. Brown, Combust. Flame 82 (1990) 312–333.
[23] J.A. Miller, C.T. Bowman, Prog. Energy Combust. Sci. 15 (1989) 287–338.
[24] O.P. Korobeinichev, A.G. Shmakov, I.V. Rybitskaya, T.A. Bolshova, D.A. Chernov, D.A. Knyazkov, A.A. Konnov, Kinet. Catal. 50 (2) (2009) 156–161 (translated from Kinetika i Kataliz 50 (2) (2009) 170–175).
[25] F.H.V. Coppens, J. De Ruyck, A.A. Konnov, Combust. Flame 149 (2007) 409–417.
[26] L.P.H. de Goey, A. Van Maaren, R.M. Quax, Combust. Sci. Technol. 92 (1993) 201–207.
[27] A. Van Maaren, D.S. Thung, L.P.H. de Goey, Combust. Sci. Technol. 96 (1994) 327–344.
[28] I.V. Rybitskaya, A.G. Shmakov, V.M. Shvartsberg, O.P. Korobeinichev, Combust. Explos. Shock Waves 44 (2008) 133–140.
[29] R.T.E. Hermanns, A.A. Konnov, R.J.M. Bastiaans, L.P.H. de Goey, Energy Fuels 21 (2007) 1977–1981.
[30] O.P. Korobeinichev, S.B. Il'in, V.V. Mokrushin, A.G. Shmakov, Combust. Sci. Technol. 117 (1–6) (1996) 51–67.
[31] O.P. Korobeinichev, S.B. Ilyin, V.M. Shvartsberg, A.A. Chernov, Combust. Flame 118 (4) (1999) 718–726.
[32] J. Warnatz, Combust. Sci. Technol. 26 (5) (1981) 203–213.
[33] O.P. Korobeinichev, A.G. Tereshchenko, I.D. Emel'yanov, A.L. Rudnitskii, S.Y. Fedorov, L.V. Kuibida, V.V. Lotov, Combust. Explos. Shock Waves 21 (1985) 524–530.
[34] W.E. Kaskan, Proc. Combust. Inst. 6 (1957) 134–141.
[35] V.V. Dubinin, B.Y. Kolesnikov, G.I. Ksandopulo, Combust. Explos. Shock Waves 13 (6) (1977) 785–788.
[36] T. Turanyi, I.G. Zsely, C. Frouzakis, KINALC: a CHEMKIN based program for kinetic analysis. <http://www.chem.leeds.ac.uk/Combustion/Combustion.html>.
[37] T. Turanyi, MECHMOD v. 1.4: program for the transformation of kinetic mechanisms. <http://www.chem.leeds.ac.uk/Combustion/Combustion.html>.
[38] I.G. Zsely, I. Virag, T. Turanyi, Flux viewer: visualisation tool for element fluxes. <http://garfield.chem.elte.hu/Combustion/fluxviewer.htm>.
[39] M. Rohrig, H.G. Wagner, Proc. Combust. Inst. 25 (1994) 975–981.
[40] P. Glarborg, P.G. Kristensen, K. Dam-Johansen, M.U. Alzueta, A. Millera, R. Bilbao, Energy Fuels 14 (4) (2000) 828–838.
[41] P. Dagaut, F. Lecomte, J. Mieritz, P. Glarborg, Int. J. Chem. Kinet. 35 (11) (2003) 564–575.
[42] J.C. Mackie, G.B. Bacskay, J. Phys. Chem. A 109 (2005) 11967–11974.
[43] A. Fontijn, S.M. Shamsuddin, D. Crammond, P. Marshall, W.R. Anderson, Combust. Flame 145 (3) (2006) 543–551.
[44] D.L. Baulch, C.J. Cobos, R.A. Cox, P. Frank, G. Hayman, Th. Just, J.A. Kerr, T. Murrells, M.J. Pilling, J. Troe, R.W. Walker, J. Warnatz, Summary table of evaluated kinetic data for combustion modelling: supplement 1, Combust. Flame 98 (1994) 59–79.
[45] B.S. Haynes, Combust. Flame 28 (1977) 81–91.